LUND UNIVERSITY

Non-radiative decay and fragmentation in water molecules after $1a_1^{-1}4a_1$ excitation and core ionization studied by electron-energy-resolved electron-ion coincidence spectroscopy

Sankari, Anna; Stråhlman, Christian; Sankari, Rami; Partanen, Leena; Laksman, Joakim; Kettunen, J. Antti; Galván, Ignacio Fdez; Lindh, Roland; Malmqvist, Per Åke; Sorensen, Stacey L.

LUND UNIVERSITY

PO Box 117
221 00 Lund
+46 46-222 00 00

Non-radiative decay and fragmentation in water molecules after $1a_1^{-1}4a_1$ excitation and core ionization studied by electron-energy-resolved electron–ion coincidence spectroscopy

Anna Sankari,[1,2] Christian Stråhlman,[3,4] Rami Sankari,[4,5] Leena Partanen,[6,5] Joakim Laksman,[1,4] J. Antti Kettunen,[6] Ignacio Fdez. Galván,[7] Roland Lindh,[7] Per-Åke Malmqvist,[2] and Stacey L. Sorensen[1]

[1]*Dept. of Physics, Lund University,*
P.O. Box 118, S-22100 Lund, Sweden
[2]*Dept. of Theoretical Chemistry, Lund University,*
Chemical Center, P.O. Box 124, S-22100 Lund, Sweden
[3]*Dept. of Materials Science and Applied Mathematics,*
*Malmö University, S-20506 Malmö, Sweden**
[4]*MAX IV Laboratory, Lund University,*
P.O. Box 118, S-22100 Lund, Sweden
[5]*Dept. of Physics, Tampere University of Technology,*
P.O. Box 692, FIN-33101 Tampere, Finland
[6]*Dept. of Physics, P.O. Box 3000,*
FIN-90014 University of Oulu, Oulu, Finland
[7]*Dept. of Chemistry – BMC, Uppsala University,*
P.O. Box 576, S-75123 Uppsala, Sweden

(Dated: May 31, 2021)

Abstract

In this paper we examine the decay and fragmentation of the core-excited and core-ionized water molecule combining quantum chemical calculations and electron-energy-resolved electron–ion coincidence spectroscopy (PEPICO). The experimental technique allows us to connect electronic decay from core-excited states, electronic transitions between ionic states, and dissociation of the molecular ion. To this end, we calculate the minimum energy dissociation path of the core-excited molecule and the potential energy surfaces of the molecular ion. Our measurements highlight the role of ultra-fast nuclear motion in the $1a_1^{-1}4a_1$ core-excited molecule in the production of fragment ions. OH^+ fragments dominate for spectator Auger decay. Complete atomization after sequential fragmentation is also evident through detection of slow H^+ fragments. Additional measurements of the non-resonant Auger decay of the core-ionized molecule $(1a_1^{-1})$ to the lower-energy dication states show that the formation of the $OH^+ + H^+$ ion pair dominates, whereas sequential fragmentation $OH^+ + H^+ \rightarrow O + H^+ + H^+$ is observed for transitions to higher dication states, supporting previous theoretical investigations.

*Electronic address: `christian.strahlman@mau.se`

I. INTRODUCTION

The properties of water and of the water molecule are fundamental to understanding a plethora of different chemical processes. In particular, studies of processes involving x-ray absorption have provided deep insights into the dynamics of the isolated water molecule. Core-excited water molecules revealed nuclear dynamics on the fs time scale, thus competing with electronic decay of the core-hole state. While x-ray absorption excites the molecule, subsequent electronic decay can map out the highly rapid evolution of the system. Both resonant inelastic x-ray scattering and resonant Auger spectroscopy are powerful tools for monitoring the development of the system as the wave packet evolves on the excited-state potential energy surface [1–5]. The latter technique was used by Hjelte *et al.* [4]. They observed resonant Auger decay arising from the molecular fragment, thus evidencing ultrafast dissociation when the photon energy is tuned through the $1a_1^{-1}4a_1$ resonance.

This study aims to investigate electronic and nuclear dynamics of the water molecule after core excitation to the LUMO as well as a core ionization. Core excitation and ionization can be induced by soft x-rays promoting one of the electrons in the $1a_1$ core orbital to an unoccupied molecular orbital (excitation) or to the vacuum level (ionization). The excited molecule is very unstable and decays on a fs time scale through electron emission [3, 6] or photon emission [7, 8]. Decay through electron emission—(resonant) Auger decay—is the dominating channel.

Electronic decay also competes with nuclear dynamics on the fs time scale. Especially in the case of excitation to the $4a_1$ orbital, both resonant inelastic x-ray scattering (RIXS) [2] and resonant Auger electron spectroscopy (RAES) [4] have shown that ultra-fast dissociation takes place within the core-hole lifetime, which for oxygen is less than 5 fs. Ultra-fast dissociation implies that the core-excited H_2O^* molecule dissociates to $OH^* + H$ before resonant Auger decay, which then takes place in the OH^* fragment. The probability of ultra-fast dissociation after core excitation to the $4a_1$ orbital was estimated to be as large as 30% [9]. Theoretical investigations of this process have also been presented [5, 10, 11].

Nuclear motion leading to fragmentation of the water molecule also happens in the ionic final states. The fragmentation of such valence-excited ionic states has been extensively studied, both experimentally [12–14] and theoretically [10, 11, 15, 16]. Accordingly, complete understanding of the excited molecule and the subsequent decay and fragmentation

must combine measuring the electronic decay and understanding the nuclear dynamics on potential energy surfaces both before and after electronic decay.

This study combines investigation of decay and dynamics of core-excited and -ionized molecules by means of electron-energy-resolved photoelectron photoion coincidence spectroscopy (PEPICO). This allows us to connect two fundamental outcomes of the decay process: the kinetic energies of (resonant) Auger electrons and the ion fragments produced from the same event, linking the dynamics of the excited and final states. Measured resonant [3, 4] and normal [6, 17] Auger electron spectra have been presented in previous studies. Partial ion yields in the core-electron resonant region have also been measured [18]. In addition, the dynamics of the fragmentation of the core-excited molecule has been studied by ion momentum imaging [19]. However, coincidence studies on water have to our knowledge only been performed following VUV excitation [13, 20].

In addition to PEPICO measurements, we performed quantum-chemical calculations of the potential energy surfaces of the core-excited and core-ionized states in order to interpret the results. The calculations help to understand the effect of the nuclear motion. Moreover, the combined experiments and calculations allow us to chart in detail the three-step process involving movement on the core-excited energy surface, electronic decay, and subsequent movement and decay in ionic states.

II. EXPERIMENT

The photoelectron photoion coincidence (PEPICO) experimental station has been described in detail in previous studies [21]. The system consists of a modified Scienta SES-100 hemispherical deflection analyzer [22] for electron analysis. The original CCD detector was replaced by a resistive-anode detector, Quantar model 3394A, for fast electron detection required by coincidence studies. A Wiley–McLaren type [23] time-of-flight mass spectrometer (TOFMS) was used for ion detection [24]. This TOFMS has a narrow extraction region, and due to the delay between ion creation and the extraction pulse, ions with high kinetic energies escape the source region before they are extracted towards the ion detector. The lightest ion, H^+, is thus likely to escape detection more often than heavier fragments, such as O^+ and OH^+. The heavier fragments carry less kinetic energy due to momentum conservation. Electrostatic simulations with SIMION [25] showed that positive ions with isotropic velocity

4

distribution had reduced transmission through the TOFMS starting from 2 eV kinetic energy and for 10 eV ions was reduced to 9%. Ion branching ratios are affected by this reduction and are thus not reliable as absolute measures. A comparison of the full (non-coincident) electron spectrum to the coincidence spectrum, i.e., those electrons that come in coincidence with at least one ion, exhibits significant differences when transmission of the relevant ion is low. Therefore, larger differences become an indirect indicator of production of fast H^+ ions. (In general, about 1 in 50 electrons are detected in coincidence with an ion.)

The experiments were performed at the MAX IV Laboratory in Lund, Sweden, at the (now decommissioned) I411 beamline [26] located on the MAX II storage ring. The beamline was equipped with a SX700 plane grating monochromator and operated in the photon energy range 50–1500 eV. The hemispherical electron analyzer and the ion TOFMS were mounted facing each other, perpendicular to the photon beam, at the magic angle with respect to the linearly polarized synchrotron radiation. For resonant Auger measurements, the photon energy was tuned to the O $1s \rightarrow 4a_1$ resonance at 534.0 eV. The normal Auger measurements were performed at 550.0 eV photon energy. The beamline exit slit was set to 60 μm, corresponding to approximately 640 meV photon bandwidth. As the pass-energy of the hemispherical electron analyzer was 200 eV, its resolution was approximately 3 eV. The electron spectra were calibrated in two steps. The detector's energy dispersion was established by using H_2O valence photoelectron lines [27]. Secondly, the absolute values of the kinetic energies of the resonant Auger electrons were found by comparing the spectrum to the high-resolution resonant Auger spectrum measured by Hjelte *et al.* [4] at the O $1s \rightarrow 4a_1$ resonance maximum at 534.0 eV. The normal Auger electron spectrum was calibrated using the energies from the experimental study by Moddeman *et al.* [17]. Calculated energies were shifted 2.5 eV towards higher energies (corresponding to less than 0.6 % of the kinetic energy).

Water vapor was introduced to the sample area through a capillary, increasing the chamber pressure to $2.5 \cdot 10^{-6}$ mbar. The capillary tip was aligned to the beam to ensure maximum pressure in the sample area (estimated to be 10–50 times higher than the chamber pressure). The deionized liquid water sample was connected to a gas inlet system. Before leaking the gas into the chamber, the gas inlet was cleaned by repeated freeze–pump–thaw cycles. The vapor pressure of the water sample was sufficient to provide a steady flow through the capillary during the experiments.

The coincidence data were acquired by collecting TOFMS detector signals, which act as a stop, following a start pulse originating from either an electron detection or a random trigger from a pulse generator. These coincidence events contain information about the kinetic energy of an observed electron and the ion time-of-flight data. With this setup, up to four ions arriving in coincidence with the electron can be recorded. The TOFMS was operated in the pulsed mode so that for every start trigger, whether it is an electron or a random trigger, the ions' time-of-flight was measured. Thus, an electron-energy-resolved coincidence spectrum was obtained at the same time as the non-coincident ion mass spectrum provided by the random triggers. With suitable normalization, as described in Ref. [21], the non-coincident spectrum can be subtracted from the coincidence spectrum, which removes the contributions from accidental coincidences. This methodology was employed in the production of the PEPICO maps and coincident ion yields (CIYs) in this paper.

III.   CALCULATIONS

We designed quantum chemical calculations to simulate the core-excited and -ionic potential surfaces of water. We used the atomic natural orbital basis sets (ANO-RCC), which are relativistic contractions of the ANO-L basis set [28]. We made relativistic corrections using the second order Douglas–Kroll–Hess transformed Hamiltonian [29, 30]. The core-excited states of the water molecule have a mixed valence and Rydberg character. Therefore, we modified the oxygen ANO-RCC basis set by supplementing two s, two p, and one d diffuse functions placed at the oxygen atom position as described by Rubio, Serrano-Andrés, and Merchán [31]. Energies for the ground, ionized, excited, and final (di)cation states were calculated based on multireference second-order perturbation theory using a restricted active space self-consistent field (SCF) wave function as reference—RASPT2/RASSCF [32]. The RASSCF is a multiconfigurational SCF method, but since the RASSCF energies lack dynamic correlation, it is added using perturbation theory in a subsequent calculation using RASPT2. We assume that the Born–Oppenheimer approximation is valid, i.e., the ionization or excitation process is much faster than nuclear motion. Therefore, the starting geometry of the molecule chosen after excitation or ionization is the same as for the ground state. The Born–Oppenheimer approximation also applies to the Auger process, where we assume that the geometry of the resulting ion is identical to that of the core-excited molecule.

In the ground state, the water molecule has C_{2v} symmetry with an O–H bond length of 0.957 Å and an H–O–H angle of 104.5° [33]. This symmetrical geometry was used as the starting point, but since the core-excited state dissociates asymmetrically by elongation of one O–H bond [2, 4], we introduced a slight asymmetry ($r_1 = 0.9570$ Å, $r_2 = 0.9573$ Å) in order to avoid artificial preservation of symmetry in the geometry optimization. The calculations presented in this paper were performed using the MOLCAS quantum chemistry package [34].

A. Resonant Auger spectrum

Excitation of the core electron to the $4a_1$ orbital initiates an ultra-fast dissociation process, where one hydrogen atom is separated from the core-excited OH fragment [4]. We used the SLAPAF module of MOLCAS package to optimize the geometry. The active space consisted of 10 electrons in 11 active orbitals. Within this configuration space, we obtained the orbitals by minimizing the average energy of the selected states, defined by configuration interaction (CI). We then computed the nuclear motion in the $1a_1^{-1}4a_1$ state by following the minimum energy path along the potential energy surface. The result is shown in the top panel of Fig. 1. At step 5, where the O–H bond distance of the dissociating hydrogen atom is larger than 2 Å, we consider the O–H bond to be completely dissociated.

The dominant de-excitation process is Auger decay. Since ultra-fast dissociation and Auger decay compete on the fs time scale, Auger decay can take place at any point during the dissociation. Within the Born–Oppenheimer approximation, the kinetic energy of the emitted electron corresponds to the energy difference between the core-excited state and the final ionic state—with the same geometry at that moment. We have therefore calculated the energies of some final ionic states for the geometries along the minimum energy path. These are shown in the bottom panel of Fig. 1.

B. Auger spectrum

The vibrational structure observed in the O $1s$ photoelectron spectrum of water [35] is a signature of the bonding character of the core-ionized state. Indeed, calculations of the nuclear dynamics after single core-electron ionization in water show only a bending vibra-

TABLE I: Calculated Auger electron energies resulting from decay to the dominant final dication states (H_2O^{2+}). They are compared with previous calculations by Inhester $et\ al.$ [36]. Our calculated energies are also shown in Fig. 4.

State		Energy (eV)	Energy (eV) [36]
$1b_1^{-2}$	$^1A_1$	499.4	499.39
$3a_1^{-1}1b_1^{-1}$	$^1B_1$	498.8	497.98
$3a_1^{-2}$	$^1A_1$	496.1	494.64
$1b_2^{-1}1b_1^{-1}$	$^1A_2$	493.7	494.68
$3a_1^{-1}1b_2^{-1}$	$^1B_2$	492.2	492.36
$1b_2^{-2}$	$^1A_1$	485.4	487.45

tional mode [36]. Therefore, no dissociation is expected prior to Auger decay. Nevertheless, a small degree of nuclear motion is expected during the core-hole lifetime.

We examined the behavior of the core-hole state $1a_1^{-1}$ by distributing the 9 electrons among 11 active orbitals, with the added restriction that (at most) one electron occupies the $1a_1$ orbital. Optimization of the core-hole state geometry indicates a slight increase in bond length ($r_1 = 0.9595$ Å, $r_2 = 0.9592$ Å) and opening of the angle (122.5°) in accordance with previous calculations (listed in Tab. 1 of Ref. [35] and shown by Ref. [36]). We expect the Auger process to take place within this optimized geometry. Therefore, we calculated the energies of a number of dication states in this geometry and used the resulting H_2O^{2+} energies to calculate transition energies to these dication states. The calculated transition energies for $singlet$ states are shown in Tab. I and are compared with the energies calculated by Inhester $et\ al.$ [36]. The $triplet$ states were omitted in our calculations, since the previously calculated transition probabilities [36, 37] show that triplet states only exhibit observable intensities around 478–482 eV, which is out of the observed energy range in this work.

IV. RESULTS AND DISCUSSION

We present and discuss the experimental and theoretical results in two subsections. The first section focuses on the resonant Auger decay (i.e., from the core-excited state), while the second focuses on Auger decay (i.e., from the core-ionized molecule).

A.   Resonant Auger decay

The experimental data is presented in Fig. 2 as a PEPICO map. The right-hand-side TOF spectrum only show coincident ions. Notably, we did not observe any O^{2+} ions in coincidence with electrons, whereas O^{2+} was observed in non-coincident ion TOF at this photon energy [18]. The H_2^+ fragment was not detected in our study, but was measured in previous studies [19]. Coincident ion yields (CIYs) for all detected fragments are shown in the left-side panels.

The main decay pathways are schematically illustrated in Fig. 3 together with the fragmentation patterns following excitation to the anti-bonding state. Upon excitation to the anti-bonding state an asymmetric bond elongation is initiated along the minimum energy path on the potential energy surface. The geometry of the molecule is expected to change along the minimum energy path, as described above. If the resonant Auger decay is prompt, the molecule can decay to a bonding ion final state (case 1). The decay produces an H_2O^+ ion and a resonant Auger electron with high kinetic energy. If the Auger process happens slightly later, the distorted molecule can still decay to a bonding ion state (case 2), also resulting in a H_2O^+ ion. However, in this case the energy of the resonant Auger electron would be slightly lower. Case 3 illustrates decay to an anti-bonding ion state. In this case, dissociation continues in the final state, as predicted by its potential energy surface, primarily resulting in an OH^+ + H ensemble. Case 4 illustrates a resonant Auger decay where the core-excited molecule dissociates into an OH^* + H pair prior to electronic decay. The result is then primarily an OH^+ + H pair. This case is identical to the ultra-fast dissociation of core-excited molecules [4]. We will refer to these cases when discussing the experimental results.

Note that we expect the parent H_2O^+ ion in coincidence with electrons at 521 eV, corresponding to the prompt decay to the lowest ion $1b_1^{-1}$ state [3]. Our measurement range does not include these higher energy electrons. In region I we observe only the H_2O^+ parent ion. One possibility in this energy range is prompt decay to the bonding $3a_1^{-1}$ ion state (case 1). Another is later decay to the bonding $1b_2^{-1}$ ion state (case 2). We conclude from looking at the calculated potential energy surfaces for ionic states in Fig. 1 that decay to one of the two lowest-energy states is the only energetically possible process. Coincident detection with the parent H_2O^+ ion is consistent with the calculations.

9

In region II at 514–517 eV both the parent H_2O^+ ion and the OH^+ fragment are observed. The appearance of the parent ion can be explained by a combination of prompt decay to the third-lowest bonding $1b_2^{-1}$ ion state (case 1) and later decay to the $3a_1^{-1}$ ion state (case 2). Although it is not possible to access anti-bonding ion states in this energy range, we observe also OH^+, O^+ and even H^+ ions in this region. The appearance energy for the OH^+ fragment is 18.01 eV [38]. In our experiment the equivalent process would be electrons with 516 eV kinetic energy or less measured in coincidence with OH^+ for 534.0 eV excitation energy. Therefore, the appearance of OH^+ is energetically possible in region II if a suitable decay pathway exists. Indeed, direct valence ionization studies [13, 38] show that OH^+ fragments result from dissociation of the $1b_2^{-1}$ ion state. The mechanism for forming the OH^+ + H pair has been studied in detail by Suárez, Méndez and Rabadán [16]. They show that there is fast transfer (less than 10 fs) from the $1b_2^{-1}$ to the $3a_1^{-1}$ state through a conical intersection, while a much slower transfer (several ps) from the $3a_1^{-1}$ to the $1b_1^{-1}$ state takes place due to Renner–Teller coupling. The $1b_1^{-1}$ ground state may dissociate to OH^+ + H. Our observation of OH^+ in region II as well as the decrease of parent ion signal at lower electron energies is therefore in good agreement with a prompt resonant Auger decay to the ion $1b_2^{-1}$ state. In addition, dissociation of the vibrationally-excited $3a_1^{-1}$ state leads to production of H^+. Although the H^+ ion yield is weak in region II, our data hints at an increase in H^+ production in this region. The weakness of this channel was also discussed by Suárez, Méndez and Rabadán. They argued that the larger experimental cross-section for production of OH^+ indicates that fragmentation through the $1b_1^{-1}$ state is larger than via the $3a_1^{-1}$ state.

Between 510 eV and 512 eV (region III), we see a large increase in both electrons and OH^+ fragments. Hjelte *et al.* [4] showed that several features in the resulting resonant Auger decay spectrum result from ultra-fast dissociation, which was attributed to the OH^* fragment, i.e., case 4. Indeed, if the core-excited OH^* + H ensemble is created at 531 eV excess energy, this would involve transitions to fragment ionic states with binding energies between 19 eV and 21 eV. Stranges *et al.* measured the inner-shell absorption spectrum of neutral OH and extracted spectroscopic parameters for the $^2\Sigma^+$ core-excited state [39]. The vertical energy is 525.8 eV. Hirst and Guest calculated the energy of ionic states in the valence region [40], and Katsumata and Lloyd measured the binding energy of the first ionic state at 13.0 eV [41]. Using these values, we expect the highest energy feature in the OH

resonant Auger energy spectrum to be at approximately 512.8 eV. For vibrationally excited OH* fragments, the "hot band" would result in a slightly higher kinetic energy—513.4 eV. These values agree with the calculation presented by Hjelte *et al.* [4] and closely match the energy of the experimental feature in region II.

It is not possible to determine whether the dissociation seen in region III takes place in the core-excited state or in the final ionic state from the experimental data alone. Nevertheless, the energies of the potential energy surfaces in Fig. 1 support the claim that the OH$^+$ ions in the region 510–512 eV practically all result from ultra-fast dissociation in the core-excited state. There are no accessible final states for the non-dissociated molecule in this range.

In region IV, we reach higher anti-bonding spectator resonant Auger final states in both early and late resonant Auger decay, while remaining below the double ionization threshold (31.6 eV [42], corresponding to kinetic energy 502.4 eV). The amount of OH$^+$ decreases, and complete atomization resulting in O$^+$ is evident. The O$^+$ fragment appearance energy is 18.7 eV [38]. However, Hult Roos *et al.* [13] observed only a very weak O$^+$ yield at this energy. Therefore, the O$^+$ production must also be the result of decay to anti-bonding spectator resonant Auger final states. We also observe light H$^+$ ions with practically zero kinetic energy, indicating a sequential dissociation to $O + H^+_{slow} + H_{fast}$.

Below 502.4 eV (region V), it is energetically possible to create an ion pair. In addition, the participator $2a_1^{-1}$ state is reached. According to our calculations, only prompt resonant Auger transitions to spectator final states or to the $2a_1^{-1}$ final state can produce these electron energies. The possible spectator final states are strongly repulsive, and high kinetic energies of fragments are expected. The presence of both O$^+$ and H$^+$ ions is again a sign of sequential fragmentation leading to a complete atomization, where the first hydrogen (either H or H$^+$) leaving the parent ion will carry away most of the kinetic energy released.

B. Ion-Auger electron coincidence spectra

The experimental data is presented as a PEPICO map in Fig. 4. Core-electron ionization followed by the emission of an Auger electron creates a rapidly dissociating dication due to Coulomb repulsion. Indeed, Piancastelli *et al.* [18] did not detect the parent H$_2$O^{2+} ion in their study near the O 1s ionization threshold. Our data can be separated into three regions in the PEPICO map: A, B, and C. The dominating feature (A) in the spectrum

11

is due to Auger transitions to the $1b_1^{-2}$ and $3a_1^{-1}1b_1^{-1}$ states. According to Gervais *et al.* [43], these states dissociate into an $OH^+ + H^+$ ion pair. OH^+ is indeed observed in our experiment. As indicated above, protons, carrying most of the kinetic energy released in a Coulomb explosion, are expected to escape detection.

Events in the next region (B) are associated with Auger transitions to states in $3a_1^{-2}$, $1b_2^{-1}1b_1^{-1}$, and $1b_2^{-1}3a_1^{-1}$ configurations, observed mainly in coincidence with H^+. Given the geometry of the experimental setup, detection of any protons is strong indication of a sequential three-body break-up: This process entails the parent dication emitting a fast proton, and then the resulting OH^+ ion dissociates further into a slow $O + H^+$ pair. The absence of O^+ in this region supports this interpretation. If neutral oxygen is produced, the only possible fragmentation channel would indeed be $H_2O^{2+} \rightarrow OH^+ + H_{fast}^+ \rightarrow O + H_{slow}^+ + H_{fast}^+$.

For the $3a_1^{-2}$ state, an indication of the intermediate product (OH^+) is seen in our PEPICO map. This supports the suggestion that the $3a_1^{-2}$ final dication state can produce OH^+ fragments or an $O + H^+$ pair if the excess kinetic energy is high enough to overcome the potential well [43].

The feature seen in region C is interpreted as originating from dication triplet states with one hole in the $2a_1$ orbital [6, 36]. Gervais *et al.* [43] did not study the potential energy surfaces of these triplet states, but they predict three-body fragmentation even for low-energy triplet states. Our observation of O^+ supports the suggestion of complete atomization. Whether it is a concerted $H_2O^{2+} \rightarrow O^+ + H^+ + H$ or sequential $H_2O^{2+} \rightarrow OH^+ + H^+ \rightarrow O^+ + H^+ + H$ fragmentation is not possible to deduce in our data.

V.   CONCLUSIONS

We have studied the fragmentation of the water molecule after core excitation to the $4a_1$ orbital as well as after O $1s$ ionization. In order to chart the concerted effects of electronic decay and nuclear dynamics, we performed electron-energy-resolved photoelectron photoion coincidence (PEPICO) experiments and multi-configurational electron structure simulations.

For resonant excitation to the $1a_1^{-1}4a_1$ state, electrons in the energy range 515–520 eV are detected mainly in coincidence with H_2O^+ ions. These can be produced by decay to the $1b_2^{-1}$ and $3a_1^{-1}$ states. OH^+ fragments at 515 eV electron energy are produced by population of the

$1b_2^{-1}$ state, which dissociates via the $3a_1^{-1}$ state [16]. We have shown that electrons with 510–512 eV kinetic energy in coincidence with OH^+ fragments arise from ultra-fast dissociation before electron emission. At lower electron energies, a manifold of higher anti-bonding ion states result in complete atomization and production of both O^+ and H^+ fragments.

Electronic decay of the core-ionized molecule to the $3a_1^{-2}$, $1b_2^{-1}1b_1^{-1}$ and $1b_2^{-1}3a_1^{-1}$ states leads to a sequential fragmentation $H_2O^{2+} \rightarrow OH^+ + H_{fast}^+ \rightarrow O + H_{slow}^+ + H_{fast}^+$ evidenced by the observation of slow H^+ fragments. Decay to the lowest dication states $1b_1^{-2}$ and $3a_1^{-1}1b_1^{-1}$ leads to the formation of a $OH^+ + H^+$ ion pair.

Acknowledgments

---

[1] E. Ertan, V. Savchenko, N. Ignatova, V. Vaz da Cruz, R. C. Couto, S. Eckert, M. Fondell, M. Dantz, B. Kennedy, T. Schmitt, et al., Phys. Chem. Chem. Phys. **20**, 14384 (2018), URL http://dx.doi.org/10.1039/C8CP01807C.

[2] L. Weinhardt, A. Benkert, F. Meyer, M. Blum, R. G. Wilks, W. Yang, M. Bär, F. Reinert, and C. Heske, J. Chem. Phys. **136**, 144311 (2012).

[3] M. N. Piancastelli, B. Kempgens, U. Hergenhahn, A. Kivimäki, K. Maier, A. Rüdel, and A. M. Bradshaw, Phys. Rev. A **59**, 1336 (1999).

[4] I. Hjelte, M. N. Piancastelli, R. F. Fink, O. Bjorneholm, M. Bassler, R. Feifel, A. Giertz, H. Wang, K. Wiesner, A. Ausmees, et al., Chem. Phys. Lett. **334**, 151 (2001).

[5] O. Takahashi, M. Odelius, D. Nordlund, A. Nilsson, H. Bluhm, and L. G. M. Pettersson, The Journal of Chemical Physics **124**, 064307 (2006), URL https://doi.org/10.1063/1.2166234.

[6] H. Siegbahn, L. Asplund, and P. Kelfve, Chem. Phys. Lett. **35**, 330 (1975).

[7] S. Kashtanov, A. Augustsson, Y. Luo, J.-H. Guo, C. Såthe, J.-E. Rubensson, H. Siegbahn,

J. Nordgren, and H. Ågren, Phys. Rev. B **69**, 024201 (2004), URL `https://link.aps.org/doi/10.1103/PhysRevB.69.024201`.

[8] J. Nordgren, L. P. Werme, H. Agren, C. Nordling, and K. Siegbahn, Journal of Physics B: Atomic and Molecular Physics **8**, L18 (1975), URL `https://doi.org/10.1088%2F0022-3700%2F8%2F2%2F003`.

[9] A. Naves de Brito, R. Feifel, A. Mocellin, A. B. Machado, S. Sundin, I. Hjelte, S. L. Sorensen, and O. Bjorneholm, Chem. Phys. Lett. **309**, 377 (1999).

[10] M. Eroms, O. Vendrell, M. Jungen, H.-D. Meyer, and L. S. Cederbaum, J. Chem. Phys. **130**, 154307 (2009).

[11] M. Eroms, M. Jungen, and H.-D. Meyer, The Journal of Physical Chemistry A **116**, 11140 (2012), URL `https://doi.org/10.1021/jp304666k`.

[12] H. Ehrhardt and A. Kresling, Zeitschrift für Naturforschung A **22**, 2036 (1967), URL `https://doi.org/10.1515/zna-1967-1228`.

[13] A. H. Roos, J. H. D. Eland, J. Andersson, R. J. Squibb, and R. Feifel, The Journal of Chemical Physics **149**, 204307 (2018), https://doi.org/10.1063/1.5055593, URL `https://doi.org/10.1063/1.5055593`.

[14] J. E. Reutt, L. S. Wang, Y. T. Lee, and D. A. Shirley, The Journal of Chemical Physics **85**, 6928 (1986), https://doi.org/10.1063/1.451379, URL `https://doi.org/10.1063/1.451379`.

[15] C. F. Jackels, The Journal of Chemical Physics **72**, 4873 (1980), https://doi.org/10.1063/1.439771, URL `https://doi.org/10.1063/1.439771`.

[16] J. Suárez, L. Méndez, and I. Rabadán, The Journal of Physical Chemistry Letters **6**, 72 (2015), pMID: 26263094, https://doi.org/10.1021/jz5022894, URL `https://doi.org/10.1021/jz5022894`.

[17] W. E. Moddeman, T. A. Carlson, M. O. Krause, B. P. Pullen, and G. K. Bull, W. E. Schweitzer, J. Chem. Phys. **55**, 2317 (1971).

[18] M. N. Piancastelli, A. Hempelmann, F. Heiser, O. Gessner, A. Rudel, and U. Becker, Phys. Rev. A **59**, 300 (1999).

[19] J. Laksman, E. P. Månsson, A. Sankari, D. Céolin, M. Gisselbrecht, and S. L. Sorensen, Physical Chemistry Chemical Physics **15**, 19322 (2013), URL `https://doi.org/10.1039/c3cp52625a`.

[20] J. H. D. Eland, Chem. Phys. **11**, 41 (1975), ISSN 0301-0104, URL `http://www.`

14

sciencedirect.com/science/article/pii/030101047580036X.

[21] E. Kukk, R. Sankari, M. Huttula, A. Sankari, H. Aksela, and S. Aksela, J. Electr. Spectr. Relat. Phenom. **155**, 141 (2007).

[22] M. Huttula, S. Heinäsmäki, H. Aksela, E. Kukk, and S. Aksela, J. Electron Spectrosc. Relat. Phenom. **156-158**, 270 (2007).

[23] W. C. Wiley and I. H. McLaren, Rev. Sci. Instr. **26**, 1150 (1955).

[24] M. Huttula, M. Harkoma, E. Nommiste, and S. Aksela, Nuclear Instruments and Methods in Physics Research Section A **467-468**, 1514 (2001).

[25] D. A. Dahl, International Journal of Mass Spectrometry **200**, 3 (2000).

[26] M. Bässler, A. Ausmees, M. Jurvansuu, R. Feifel, J. O. Forsell, P. de Tarso Fonseca, A. Kivimäki, S. Sundin, S. L. Sorenson, R. Nyholm, et al., Nucl. Instrum. Methods Phys. Res., Sect. A **469**, 382 (2001).

[27] C. R. Brundle and D. W. Turner, Proc. Roy. Soc. A **307**, 27 (1968).

[28] B. O. Roos, R. Lindh, P.-A. Malmqvist, V. Veryazov, and P.-O. Widmark, J. Phys. Chem. A **108**, 2851 (2004).

[29] B. A. Hess, Phys. Rev. A **33**, 3742 (1986), URL `https://link.aps.org/doi/10.1103/PhysRevA.33.3742`.

[30] G. Jansen and B. A. Hess, Phys. Rev. A **39**, 6016 (1989), URL `https://link.aps.org/doi/10.1103/PhysRevA.39.6016`.

[31] M. Rubio, L. Serrano-Andrés, and M. Merchán, J. Chem. Phys. **128**, 104305 (2008).

[32] P.-A. Malmqvist, K. Pierloot, A. R. Moughal Shahi, C. J. Cramer, and L. Gagliardi, J. Chem. Phys. **128**, 204109 (2008).

[33] G. Herzberg, *Molecular Spectra and Molecular Structure, vol. III* (Krieger Publishing Co., Malabar, Fl. USA, 1991).

[34] F. Aquilante, L. De Vico, N. Ferré, G. Ghigo, P.-A. Malmqvist, P. Neogrády, T. B. Pedersen, M. Pitonak, M. Reiher, B. O. Roos, et al., J. Comp. Chem **31**, 224 (2010).

[35] R. Sankari, M. Ehara, H. Nakatsuji, Y. Senba, K. Hosokawa, H. Yoshida, A. De Fanis, Y. Tamenori, S. Aksela, and K. Ueda, Chem. Phys. Lett. **380**, 647 (2003).

[36] L. Inhester, C. F. Burmeister, G. Groenhof, and H. Grubmüller, J. Chem. Phys. **136**, 144304 (2012).

[37] V. Carravetta and H. Ågren, Phys. Rev. A **35**, 1022 (1987).

[38] K. Norwood, A. Ali, and C. Y. Ng, The Journal of Chemical Physics **95**, 8029 (1991), https://doi.org/10.1063/1.461334, URL `https://doi.org/10.1063/1.461334`.

[39] S. Stranges, R. Richter, and M. Alagia, The Journal of Chemical Physics **116**, 3676 (2002), https://doi.org/10.1063/1.1448283, URL `https://doi.org/10.1063/1.1448283`.

[40] D. M. Hirst and M. F. Guest, Molecular Physics **49**, 1461 (1983), URL `https://doi.org/10.1080/00268978300102071`.

[41] S. Katsumata and D. Lloyd, Chemical Physics Letters **45**, 519 (1977), ISSN 0009-2614, URL `http://www.sciencedirect.com/science/article/pii/0009261477800791`.

[42] S. Truong, A. Yencha, A. Juarez, S. Cavanagh, P. Bolognesi, and G. King, Chemical Physics Letters **474**, 41 (2009), ISSN 0009-2614, URL `http://www.sciencedirect.com/science/article/pii/S0009261409004667`.

[43] B. Gervais, E. Giglio, L. Adoui, A. Cassimi, D. Duflot, and M. E. Galassi, J. Chem. Phys. **131**, 024302 (2009).
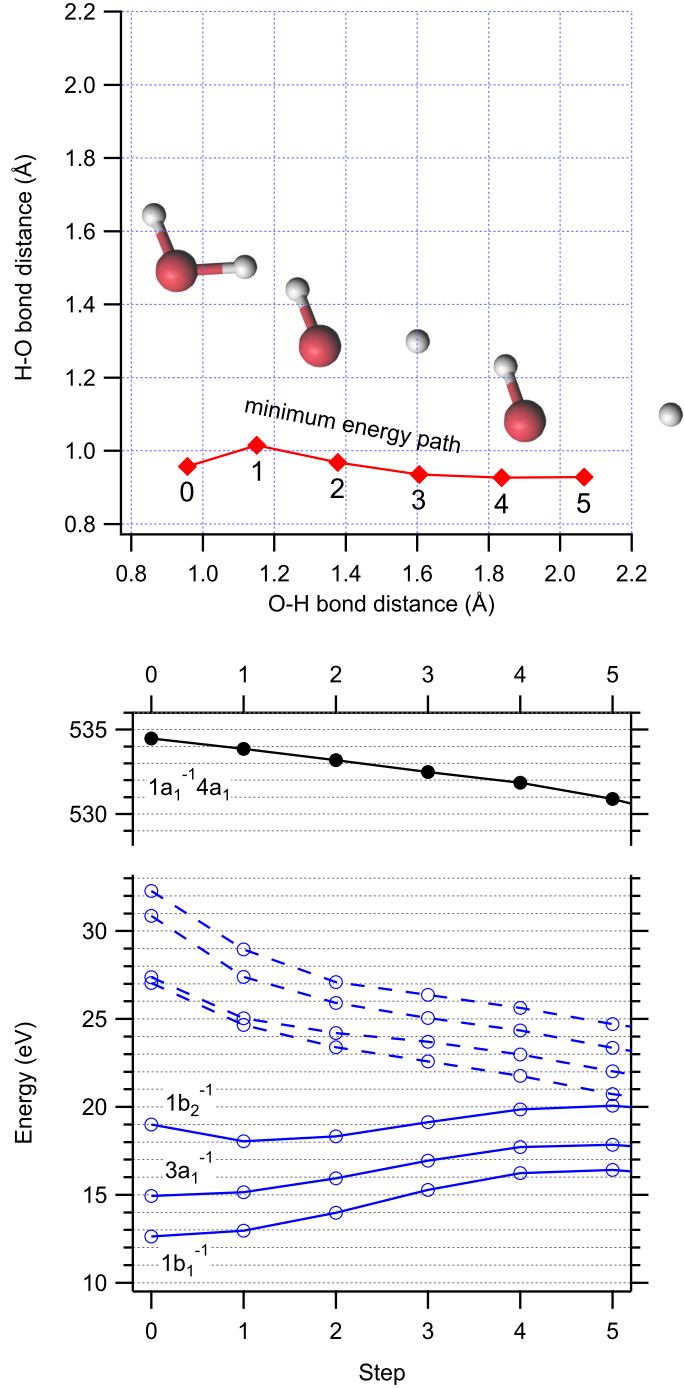
FIG. 1: Top panel: The minimum energy path along the potential energy surface of $1a_1^{-1}4a_1$ core-excited state. The x-axis and y-axis are the two bond distances, respectively. Step 0 corresponds to the (slightly distorted, see text) experimental ground-state geometry. The geometry for each step 1–5 corresponds to the geometry that has the minimum energy within a fixed hypersphere around the previous geometry. The result is an asymmetrical bond elongation. The bond angle (not displayed) changes by less than 2° from the ground-state geometry. Bottom panel: The calculated energies of the core-excited state (black line) and several ionic final states (blue lines) corresponding to steps 0–5. The three lowest ion states (solid blue lines) are the bonding $1b_1^{-1}$, $3a_1^{-1}$ and $1b_2^{-1}$ states. The higher states (dashed blue lines) are *examples* chosen from an ensemble of spectator anti-bonding ion states.
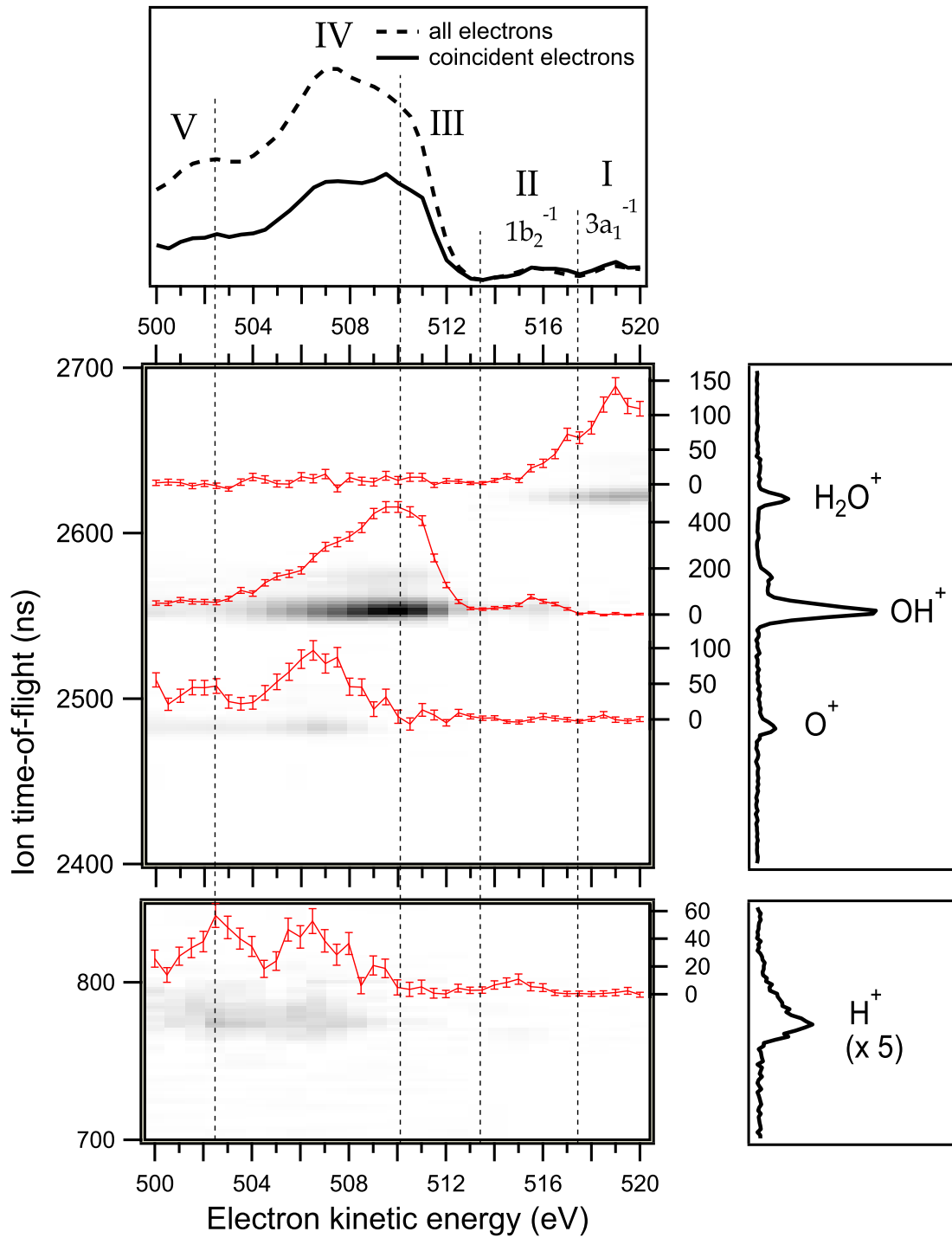
17

FIG. 2: Electron-ion coincidence map measured on top of the $4a_1$ resonance. Top panel: The resonant Auger electron spectrum showing both all electrons and those electrons detected in coincidence with ions. Right panel: The coincident ion TOF spectrum. Left panel: Electron-ion coincidence map. Solid red lines show coincident ion yields (CIY) for all fragments. The ticks for the CIYs are arbitrary, but comparable, units.
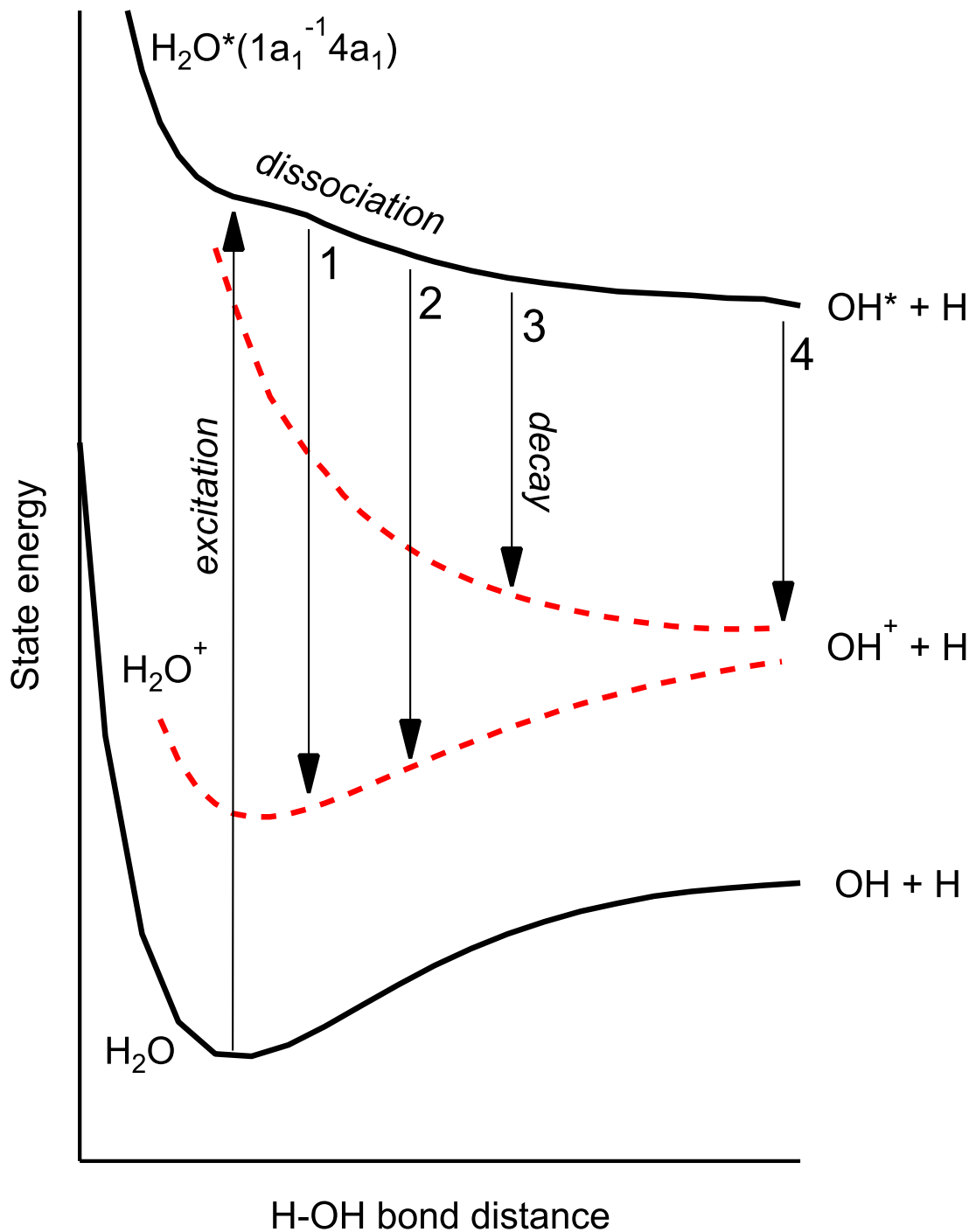
FIG. 3: A schematic illustration of the excitation, dissociation, and possible resonant Auger decay channels. The neutral ground state and the neutral core-excited state are shown with black lines, while H_2O^+ states are shown with red dashed lines. The molecule is excited from the H_2O ground state to the core-excited $H_2O^*(1a_1^{-1}4a_1)$ state, where it starts to dissociate along the potential energy surface. The possible decay patterns are (1) prompt decay to a bonding ion H_2O^+ state, (2) later decay to a bonding ion state, (3) decay to an anti-bonding dissociative ion state, and (4) late decay where the fragmented $OH^* + H$ ensemble decays to $OH^+ + H$.
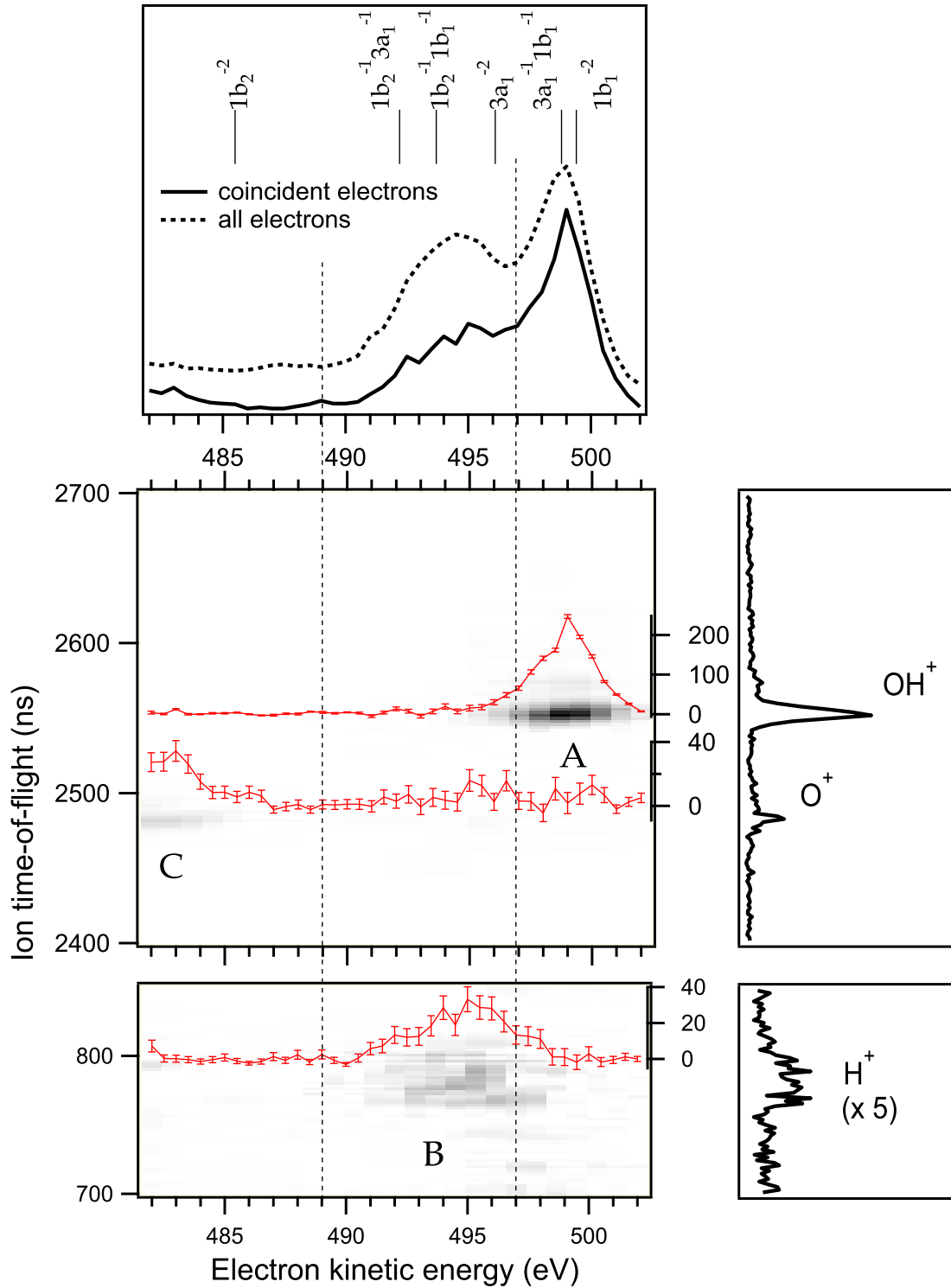
FIG. 4: Electron-ion coincidence map measured at 550 eV photon energy. Top panel: The non-resonant Auger electron spectrum showing both all electrons and those electrons detected in coincidence with ions. Calculated transition energies from the $1a_1^{-1}$ core-ionized state to the final H_2O^+ states are also shown. Right panel: The coincident ion TOF spectrum. Left panel: Electron-ion coincidence map. Solid red lines show coincidence ion yields (CIY) for all fragments. The ticks for the CIYs are arbitrary, but comparable, units.